- Supporting Information -

Diffraction of Quantum-Dots Reveals Nano-Scale Ultrafast Energy Localization

Giovanni M. Vanacore[1], Jianbo Hu[1], Wenxi Liang[1], Sergio Bietti[2], Stefano Sanguinetti[2], and Ahmed H. Zewail[1,*]

Affiliations:

[1] Physical Biology Center for Ultrafast Science and Technology, Arthur Amos Noyes Laboratory of Chemical Physics, California Institute of Technology, Pasadena, CA 91125, USA

[2] L-NESS and Dipartimento di Scienza dei Materiali, Università di Milano Bicocca, Via Cozzi 53, I-20125 Milano, Italy

*To whom correspondence should be addressed. E-mail: zewail@caltech.edu

S.1 OPTICAL ABSORPTION IN QDs

The energy per unit volume absorbed by the quantum dots upon irradiation by the pump laser has to be carefully addressed, especially when considering nanometer length scale in comparison to the bulk case[1]. The absorbed fluence, f, can be expressed as[2]:

$$f = f_0(1-R)\gamma_{QD}\frac{E_{excess}^{bulk}}{\hbar\omega} \quad (1)$$

where f_0 is the incident fluence, $\hbar\omega = 1.55$ eV (λ = 800 nm) the photon energy, R the reflection coefficient (= 0.3 for GaAs at 800 nm), γ_{QD} the absorption coefficient of the quantum dot (QD), and E_{excess}^{bulk} is the bulk (above-gap) excess energy (≈ 0.13 eV for GaAs bulk). Here, γ_{QD} can be written as:

$$\gamma_{QD} = \gamma_{bulk} f_{size}\frac{\sigma_{reson}}{\sigma_{bulk}} \quad (2)$$

where γ_{bulk} ($= 1.44 \times 10^4$ cm^{-1} in GaAs at λ = 800 nm)[3] is the bulk absorption coefficient, f_{size} is the fraction of fluence absorbed by the dot (which takes into account its reduced size compared to a bulk sample), and σ_{reson} is the enhancement factor due to resonant electronic absorption at the energy $\hbar\omega$, normalized to the bulk value σ_{bulk}; note that for QD-1, this ratio of σ is larger than one, whereas for QD-3 it is one.

In Figure S1A we depict the electron band energetics of a GaAs/$Al_{0.3}Ga_{0.7}As$ heterostructure, which induces a confinement of both electrons and holes within the dot. For GaAs at 300 K, the de Broglie wavelength of the conduction electrons is $\lambda_e = 2\pi\hbar/\sqrt{2mK_bT} \approx 30$ nm, where $T = 300$ K, $\hbar$ the Planck constant, K_b the Boltzmann constant, $m = 0.067m_0$ the electron effective mass, and m_0 is the free-electron mass. When the dot size is smaller than λ_e, quantum confinement effects become relevant, giving rise to a discrete energy spectrum and an increasing

inter-band separation, E_g, for a decreasing dot size, as shown in Figure S1B, which also displays the results of *ab initio* calculations[4,5].

The transition probability for inter-band excitation at the energy E_g can be expressed[1,6] by a Lorentzian lineshape:

$$g(\hbar\omega - E_g) = \frac{1}{\pi}\frac{(\Gamma/2)E_g}{(\hbar\omega - E_g)^2 + (\Gamma/2)^2} \quad (3)$$

giving the normalized enhancement factor for resonant absorption:

$$\frac{\sigma_{reson}}{\sigma_{bulk}}(\hbar\omega) = \frac{g(\hbar\omega - E_g)}{g(\hbar\omega - E_g^{bulk})} \quad (4)$$

In Eq. (3), $\Gamma = \hbar/\tau_L$ ($\tau_L = 120$ fs$/1.76$) is the full-width at half maximum of the inter-band transition and is associated to the interaction time between the laser and the electron distribution within the dot. It is worth noting that when the dot size increases, the energy gap E_g decreases toward the bulk value $E_g^{bulk} \approx 1.42$ eV, and thus the ratio $\sigma_{reson}/\sigma_{bulk}$ approaches the unity.

To determine the term f_{size}, it is straightforward to consider the size of the dot relative to that of the laser intensity distribution. However, we have also calculated the distribution of the electric field inside and outside the dot as induced by the incident laser. This has been obtained by means of Finite Difference Time Domain (FDTD) simulations[7] and the results are plotted in Figure S2A-F. We used the experimental bulk dielectric constants taken from the literature for both the AlGaAs substrate[8] and the GaAs dots[9]. Illumination is provided by a plane wave source and the mesh size within and around the island is 0.5 nm. Convergence is ensured by verifying that the total energy within the simulation box is 10^{-5} times smaller than that injected at the beginning of the simulation. The power absorbed by the dot is calculated as the net flux of the Poynting vector through a box surrounding it. Reference simulations were also run for a continuous film. The factor f_{size} is thus obtained by normalizing the absorption of the dot to that of the film. Further extended

simulations, using the experimentally measured inter-dot distance, confirm that no significant near-field interactions take place between neighbouring dots.

The behavior of f_{size} and $\sigma_{reson}/\sigma_{bulk}$ as a function of the dot size are shown in Figure S2G. The FDTD simulations predict that for dot dimensions smaller than the photon wavelength, the fraction, f_{size}, of laser intensity absorbed by the dot decreases for a decreasing size. On the other hand, for a decreasing dot size, the energy gap, E_g, gets closer to the photon energy, approaching the condition for a resonant electronic excitation, which is described by the relevant increase of the factor $\sigma_{reson}/\sigma_{bulk}$. This indicates that the resonances of the electronic density of states, caused by the quantum confinement, are the dominant contribution to the carriers excitation in the investigated nanostructures.

S.2 DIFFUSIVE AND NON-DIFFUSIVE REGIMES

Within the framework of the three-temperature model (3TM),[10,11] the carriers, the optical phonons, and the acoustic phonons subsystems are each in a local energetic state defined by the temperature $T_e(\boldsymbol{r},t)$, $T_O(\boldsymbol{r},t)$ and $T_A(\boldsymbol{r},t)$, respectively, where $\boldsymbol{r}=(x,y,z)$ is the spatial coordinate vector (*x* and *y* lie in the surface plane, while *z* is the direction perpendicular to it). For the case of quantum dots the differential equations involved are:

$$C_e\frac{\partial T_e}{\partial t}=\nabla\cdot(k_e\nabla T_e)-\frac{C_e}{\tau_{e-LO}}(T_e-T_O)+S(\boldsymbol{r},t) \tag{5}$$

$$C_O\frac{\partial T_O}{\partial t}=\frac{C_e}{\tau_{e-LO}}(T_e-T_O)-\frac{C_O}{\tau_{anh}}(T_O-T_A) \tag{6}$$

$$C_A\tau_R\frac{\partial^2 T_A}{\partial t^2}+C_A\frac{\partial T_A}{\partial t}=\nabla\cdot(k_A\nabla T_A)+\frac{C_O}{\tau_{anh}}(T_O-T_A)-\nabla\cdot q_b \tag{7}$$

For the substrate we can define the temperature $T_{sub}(\boldsymbol{r},t)$, which describes its lattice heating, with:

$$C_{sub}\frac{\partial T_{sub}}{\partial t} = \nabla \cdot (k_{sub}\nabla T_{sub}) \tag{8}$$

Here, $S(\boldsymbol{r}, t)$ represents the spatio-temporal profile of the laser source:

$$S(\boldsymbol{r}, t) = f\exp(-z/\chi)\frac{\mathrm{sech}^2(t/\tau_L)}{2\tau_L} \tag{9}$$

where $\chi = 694$ nm is the laser penetration depth at λ = 800 nm in GaAs,[3] and $\tau_L = 120$ fs$/1.76$. The parameters C_e, C_O, C_A and C_{sub} are the heat capacity for the electrons, the optical phonons, the acoustic phonons and the substrate subsystems, respectively.[3,12,13] The parameters k_e, k_A and k_{sub} are the thermal conductivities for electrons, acoustic phonons and substrate, respectively.3 The interaction between the three subsystems is described by the time constants: $\tau_{e-LO} = 100$ fs and $\tau_{anh} = 3.5$ ps. The first describes the coupling between the electron population and the LO optical phonons, while the latter represents the time constant for the scattering of the optical phonons with the high-energy acoustic phonons *via* the anharmonic interaction.

The term $\nabla \cdot (k_A \nabla T_A)$ describes the diffusive transport of acoustic phonons, as derived from the Fourier's law for heat conduction, while the hyperbolic term $C_A\tau_R\frac{\partial^2 T_A}{\partial t^2}$ is the Cattaneo correction[14] to a pure Fourier equation and represents the dissipative contribution to the total heat flux. The extent of energy dissipation for the high-energy acoustic phonons is reflected in the relaxation time, τ_R.[14,15] In the non-equilibrium regime, the time scale for equilibration is predicted to be proportional to the extent of the external excitation[16], meaning that the time constant τ_R would lengthen when the pump excitation fluence increases; τ_R can be expressed as the scattering time for high-energy acoustic phonons ($\tau_c \approx \Lambda_p/v_A \sim 5$ ps, where v_A is the sound velocity[17]) weighed by the population of the excited hot phonons, $\langle n_{hot}\rangle$. The population $\langle n_{hot}\rangle$ is obtained by a spectral average of the Planck distribution extended over the frequency range of the acoustic phonons created by the decay of the LO phonon for the investigated dot sizes[18].

In GaAs, the inelastic phonon mean-free path, Λ_p, for high-energy acoustic phonons, is ~ 26-27 nm. This value has been reliably obtained using two different approaches: *i*) applying the Casimir formula, as described in Ref. 3 and 19; and *ii*) as adopted in Ref. 20, by performing a spectral average of the frequency-dependent mean-free path[21] extended over the range of the acoustic phonons created by the decay of the LO phonon[18].

In the case of a ballistic (no collisions) phonon propagation, the Fourier description is incomplete and alternative approaches have to be used to describe the heat transport. The term $\nabla \cdot q_b$ within the T_A–equation (Eq. (7)) of the 3TM model represents the ballistic contribution to the transport as described within the ballistic-diffusive equation model by Chen[15], and q_b is the ballistic heat flux. Because local absorption occurs only within the dot, the created phonons transfer their energy to the substrate along the perpendicular to the interface direction (*z*-axis) since transverse dissipation of energy in the dot is not feasible. Thus, a nearly one-dimensional heat transfer along the *z*-axis is the most prominent. In this case, the ballistic term $\nabla \cdot q_b$ can be expressed within a one-dimensional geometry approximation as reported in Ref. 15. It is worth mentioning that, within Chen's model, the weight of the ballistic contribution is given by a second order exponential integral function: $E_2(z/\Lambda_p) \propto \exp(-z/\Lambda_p)$.

An alternative method to take into account the ballistic transport is the approach described by Siemens *et al.*[20]. The authors, instead of using the explicit term $\nabla \cdot q_b$, introduce a ballistic correction to the diffusive term: $1/(1+B)$, where $B \approx 2\Lambda_p/3\log(4)h$ (h is the dot height). In our case, the ballistic correction modulates both the conventional Fourier conductivity, k_A, and the Cattaneo dissipative term. The T_A–equation of the 3TM model can then be re-written as:

$$C_A \tau_R \frac{1}{1+B}\frac{\partial^2 T_A}{\partial t^2} + C_A \frac{\partial T_A}{\partial t} = \nabla \cdot \left(k_A \frac{1}{1+B} \nabla T_A\right) + \frac{C_O}{\tau_{anh}}(T_O - T_A) \qquad (10)$$

When $h \gg \Lambda_p$, $B \ll 1$ and the T_A–equation becomes purely diffusive. However, when $h \ll \Lambda_p$, $B \gg 1$ and the diffusive-dissipative terms give a negligible contribution to T_A.

It should be reminded that in the ballistic regime, the statistical distributions of the acoustic phonons is far from equilibrium, and thus the temperature T_A should be considered only as a measure of the local internal energy[15].

For dot size larger than Λ_p the ballistic term/correction becomes very small and thus the Cattaneo-Fourier terms dominate. In this case, the dynamics is mediated by the relaxation of the hot phonons and the diffusive transport. For dots smaller than Λ_p, the Fourier-Cattaneo equation over-predicts the heat flux. The introduction of the ballistic term/correction compensates this effect and the dynamics is now mainly mediated by the LO phonon decay.

In principle, an accurate description of the phonon transport in micro- and nano-scale systems should rely on the resolution of the Boltzmann transport equation (BTE). However, solving the BTE is generally difficult, although recent Monte Carlo methods[22] were introduced for this purpose. As described above, for GaAs dots a nearly one-dimensional heat transfer takes place. In this case, approximate models with *ad hoc* corrections to the heat equation have been proved to give the same accuracy as the BTE (see for instance Refs. 15 and 20). This simplified approach is the one adopted in this work, and although the results of the simulations have to be considered as a first approximation, they reproduce major features of the experimental data.

Finally, we discuss the heat transport across the interface, *S*, between the dot and the substrate. This is governed by the following energy balance:

$$\int_S \boldsymbol{n} \cdot k_A \nabla T_A = \left(1/r_{eff}\right) S (T_A - T_{sub}) \tag{11}$$

where $\boldsymbol{n}$ is the unit vector normal to the interface. In Eq. (11), r_{eff} is the effective interface thermal resistivity and can be written as: $r_{eff} = (1/k_i)(1 + B_{sub})$,[20] where k_i is the diffusive interface conductivity and $B_{sub} \propto \left(\Lambda_p^{sub}/w\right)$ is the ballistic correction[20], with Λ_p^{sub} the phonon inelastic mean-free path in the substrate and w the dot base width. However, since Λ_p^{sub} is only 4.5 nm for AlGaAs,[3,20] which is much smaller than the base width of the smallest dots (w = 31 nm for QD-1), the heat transport across the dot/substrate interface is essentially diffusive and follows a Fourier law ($r_{eff} \approx 1/k_i$)[20].

S.3 DIFFRACTION INTENSITY TRANSIENTS

In Figure S3, we present the behavior of the time constant, τ_d, of the exponential decay of the transient intensity change (see Figure 2A in the main text) as a function of the dot size and the excitation fluence for the (006), $(\bar{2}26)$, $(\bar{1}15)$ and $(\bar{3}35)$ Bragg reflections. The experimental data are shown as full symbols. For small dots (QD-1) the time constant τ_d is always $\approx$ 3.7 ps for all the Bragg spots studied and for all the fluences used. In contrast, for the large dots QD-3 τ_d exhibits a monotonic increase with the excitation fluence and a progressive decrease with the angle, δ, between the scattering vector and the [001] axis (see insets in Figure S3). The solid lines shown in Figure S3 are the results of the model described in Section S.2. A single adjustable parameter was used for the entire dataset (as a function of size, fluence and angle δ), represented by the volume-dependent phonon density of the thermal bath at the equilibrium. A satisfactory agreement with the experimental data is obtained. Further discussion is developed in the main text.

S.4 HEAT TRANSPORT ACROSS THE DOT/SUBSTRATE INTERFACE

The transient behavior on a longer time scale reveals the heat transport across the interface between the dot and the substrate. After the initial decrease, the diffraction intensity exhibits a recovery toward the equilibrium state, as displayed in Figure S4A for the $(\bar{2}26)$ Bragg spot for the three investigated dot dimensions. The recovery time, τ_r, increases for larger dot sizes: τ_r is ~ 50 ps for QD-1, ~ 150 ps for QD-2, and ~ 330 ps for QD-3. Moreover, τ_r does not depend on the scattering vector and on the excitation fluence.

As described in Section S2, at the interface phonons are diffusively scattered, making the substrate act as a thermal reservoir, whose resistance[23] is controlled by the ratio between the inelastic mean-free path of the substrate, Λ_p^{sub}, and the lateral dimension, *w*, of the dot. For AlGaAs, Λ_p^{sub} is ~ 4.5 nm and thus smaller than *w* for the investigated dots, suggesting that a diffusive transport within the substrate is expected. When only the Fourier component is included in the calculations (see Section S.2), the simulated size-dependence of the recovery time is in good agreement with the experimental data (see Figure S4B), supporting the diffusive picture. In the calculations, the diffusive interface conductivity k_i is considered as the average between the thermal conductivities of the dot and the substrate: $k_i \approx 0.5(k_A + k_{sub})$.

S.5 COHERENT OSCILLATIONS IN A HEMISPHERICAL NANOSTRUCTURE

Coherent propagation of acoustic phonons inside a confined structure can give rise to the formation of breathing oscillations of the interatomic distance. In the case of a homogeneous thin film, with thickness *d*, a standing-wave condition is valid and the frequency of the oscillations fulfills the relation $f = v/2d$, where v is the velocity of the propagating acoustic phonons.

For a nanostructure with specific geometry, where *d* is not constant, the oscillations can be obtained by dividing the structure into an infinite number of elementary volumes and then integrating the wavelet components for each of them: $\psi = \langle \sin(2\pi f(x,y)t) \rangle$, where $f(x,y) = v/2d(x,y)$, and t is the time coordinate. If the nanostructure has a symmetric shape, then $f(x,y)$ follows a Gaussian-like distribution, and thus ψ can be written as: $\psi \propto \sin(2\pi \langle f(x,y) \rangle t)$, transferring the problem to the determination of the average frequency, $\langle f \rangle$. Considering that our dots exhibit a cylindrical symmetry and can be approximated by a hemispherical shape, $\langle f \rangle$ can be written as:

$$\langle f \rangle = \frac{\int_0^{r_0} \frac{v}{2d(r)} 2\pi r dr}{\int_0^{r_0} 2\pi r dr} = \frac{v}{2} \frac{1}{\int_0^{r_0} r dr} \int_0^{r_0} \frac{r}{d_0 \sqrt{1 - \left(\frac{r}{r_0}\right)^2}} dr \quad (12)$$

where d_0 is the dot height and r_0 is the radius at the base. With the change of variable $\xi = r/r_0$, $\langle f \rangle$ can be expressed as:

$$\langle f \rangle = \frac{v}{d_0} \int_0^1 \frac{\xi}{\sqrt{1 - \xi^2}} d\xi = \frac{v}{d_0} = 2f_0 \quad (13)$$

where $f_0 \equiv v/2d_0$ is the frequency at the maximum thickness, thus obtaining the formula reported in the main text.

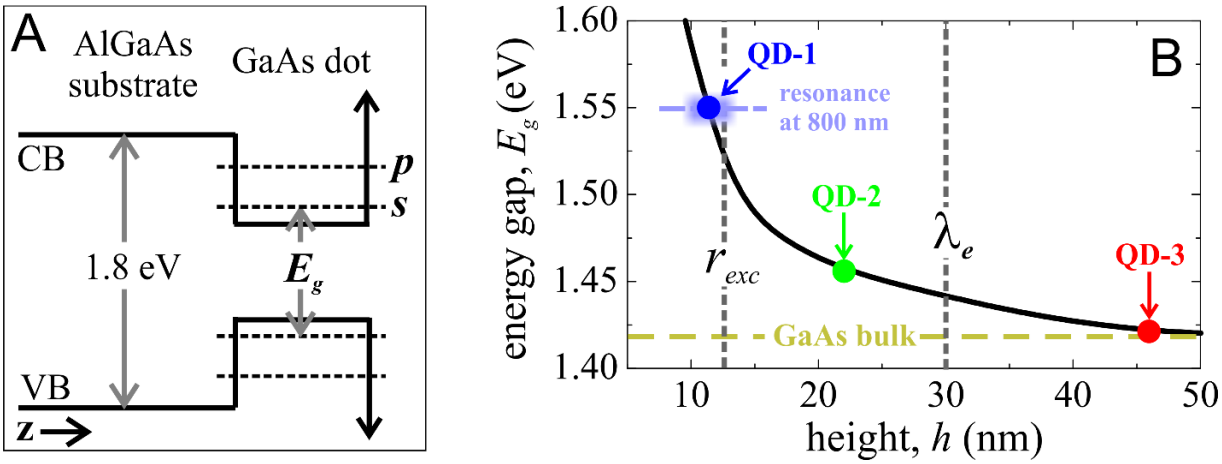

Figure S1. Electronic structure of GaAs quantum dots. **Panel A**: electron band energetics of a GaAs/$Al_{0.3}Ga_{0.7}As$ heterostructure. Both electron and holes are confined within the dot. **Panel B**: inter-band energy separation, E_g, as a function of the dot size as obtained by *ab initio* calculations; λ_e and r_{exc} represent the de Broglie wavelength of conduction electrons and the exciton radius in GaAs, respectively, which define the regimes of weak and strong quantum confinement.

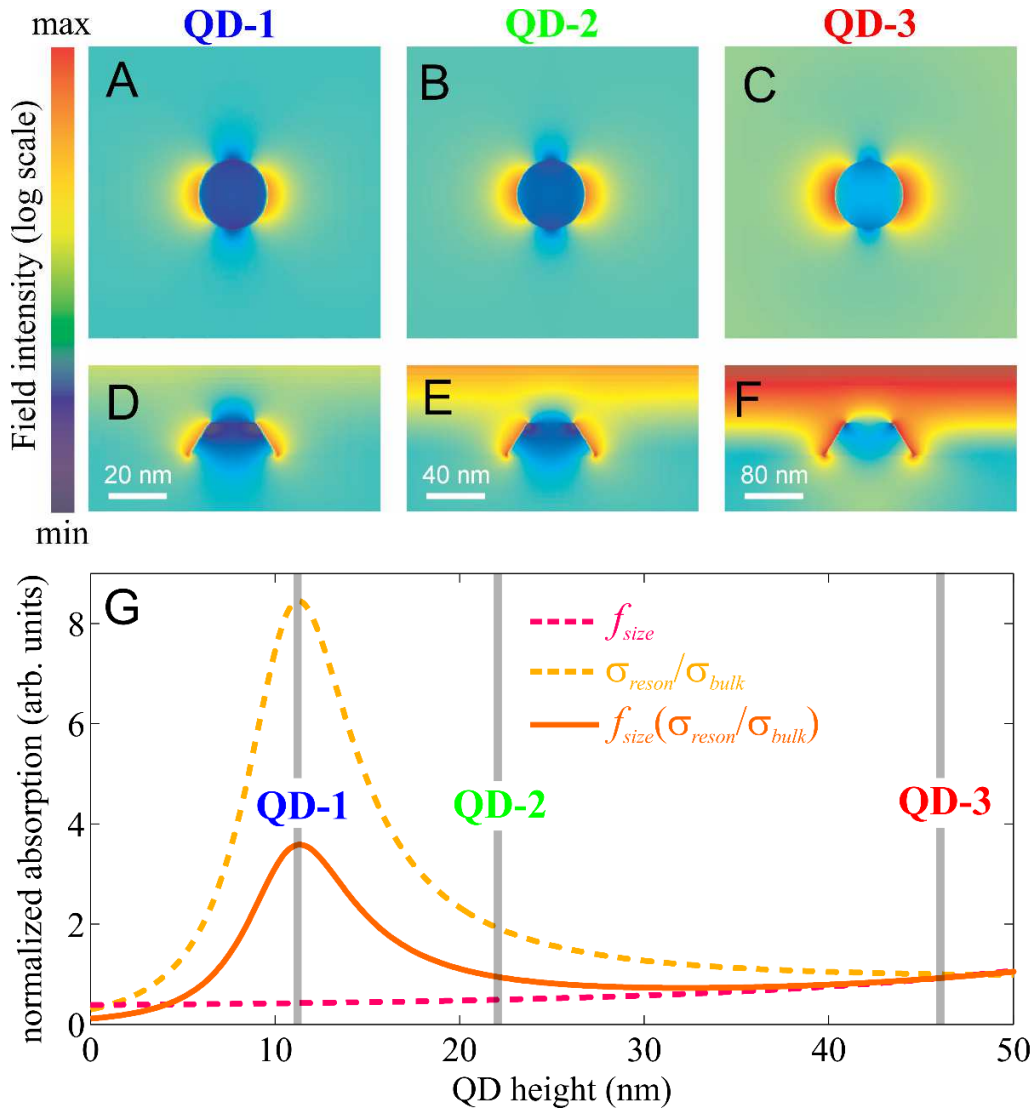

Figure S2. Optical absorption in quantum dots. **Panels A-F**: Finite Difference Time Domain (FDTD) simulations of the laser intensity distribution inside and outside the dots; panels A-D for QD-1, panels B-E for QD-2, and panels C-F for QD-3. **Panel G**: calculated behavior of the fraction of laser intensity absorbed by the dot, f_{size}, and of the enhancement factor due to resonant absorption, $\sigma_{reson}/\sigma_{bulk}$, as a function of the dot size, together with their product.

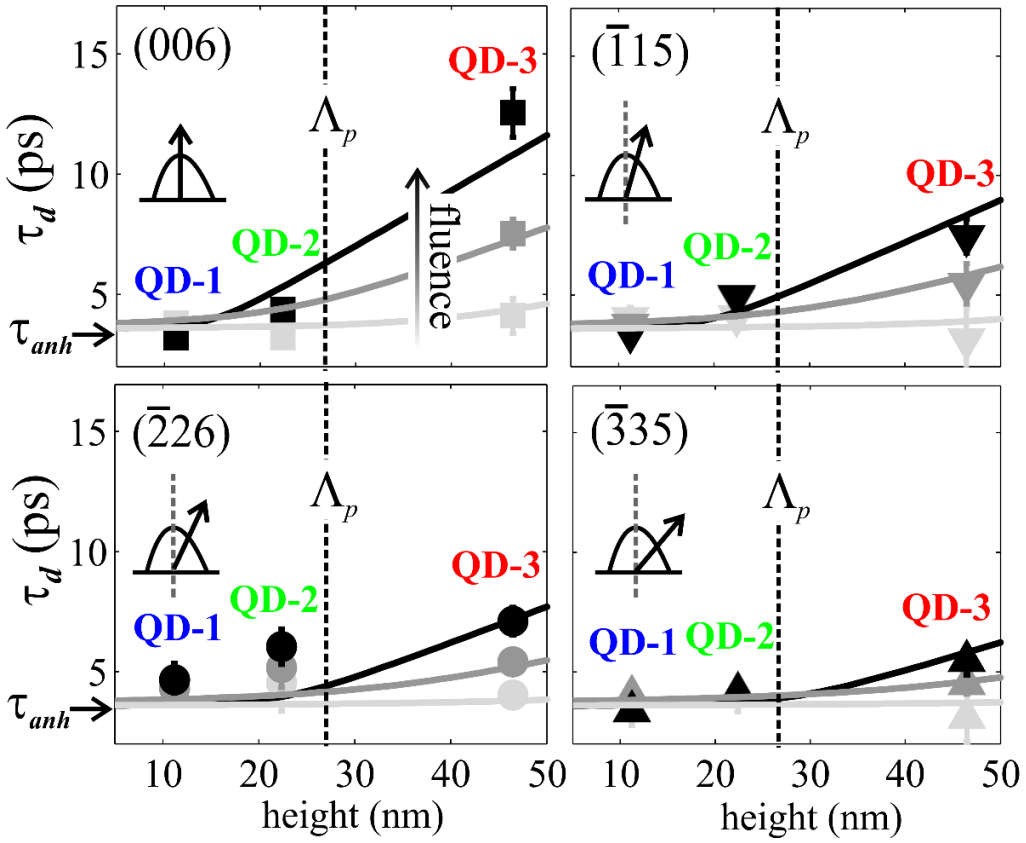

Figure S3. Time scale of structural dynamics. The experimental (full symbols) and simulated (solid lines) time constant, τ_d, is plotted as a function of the dot size and the excitation fluence for the reflections (006) (panel A), ($\bar{1}$15) (panel B), ($\bar{2}$26) (panel C), and ($\bar{3}$35) (panel D) at 4.6 mJ/cm^2 (black), 3.4 mJ/cm^2 (grey), and 2.3 mJ/cm^2 (light grey). Λ_p is the phonon inelastic mean-free path. The insets in each panel gives the direction of the scattering vector plotted in the [110] plane.

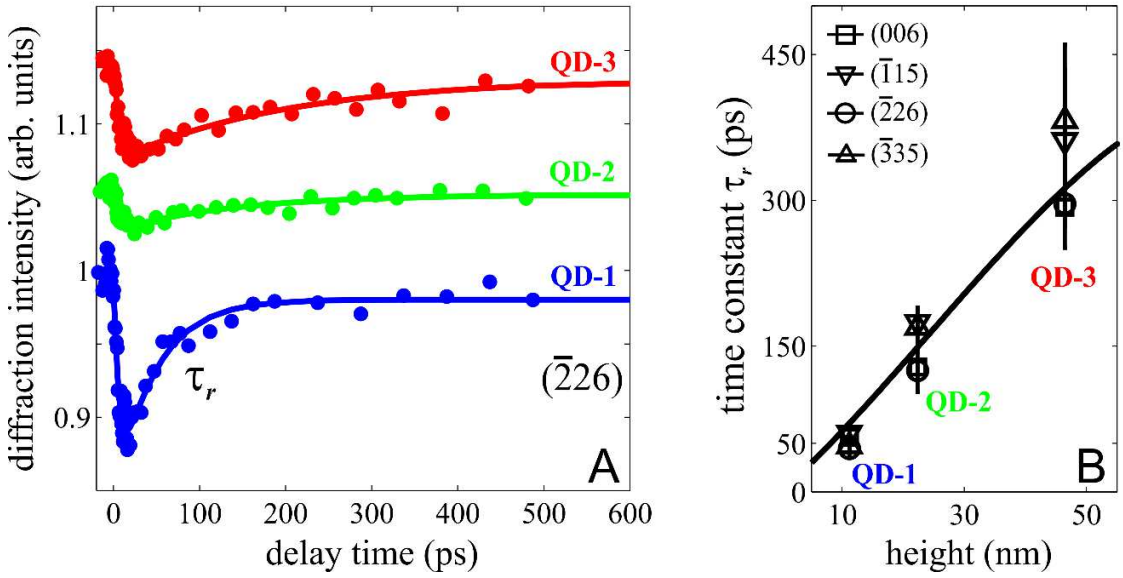

Figure S4. Recovery dynamics. **Panel A**: experimentally measured (full circles) long-time behavior of the intensity change for the $(\bar{2}26)$ Bragg spot for the three investigated dot dimensions at 4.6 mJ/cm^2; the solid lines represent the best fit of the experimental data with the combination of an exponential decay and an exponential recovery. The transients are shifted for clarity purposes. **Panel B**: size dependence of the experimentally measured (open symbols) time constant, τ_r, of the exponential recovery plotted for the reflections (006) (squares), $(\bar{1}15)$ (downward pointing triangles), $(\bar{2}26)$ (circles), and $(\bar{3}35)$ (upward pointing triangles). The black solid line represents the calculated trend of τ_r as obtained using an energy conservation balance where only a Fourier component is considered (see text for details).

REFERENCES

(1) Cardona, M.; Yu, P. *Fundamentals of Semiconductors: Physics and Material Properties*; Eds., Springer: 2010.

(2) Yang, D.-S.; Gedik, N.; Zewail, A. H. *J. Phys. Chem. C* **2007**, *111*, 4889-4919.

(3) Blakemore, J. S. *J. Appl. Phys.* **1982**, *53*, R123-R181.

(4) Marzin, J.-Y.; Bastard, G. *Solid State Commun.* **1994**, *92*, 437-442.

(5) Simulation software NEXTNANO^3 (www.nextnano.com).

(6) Accanto, N.; Minari, S.; Cavigli, L.; Bietti, S.; Isella, G.; Vinattieri, A.; Sanguinetti, S.; Gurioli, M. *Appl. Phys. Lett.* **2013**, *102*, 053109.

(7) FDTD Solutions, Version 8.5.3, Lumerical Solutions, Inc., Vancouver, BC, Canada

(8) Gehrsitz, S.; Reinhart, F. K.; Gourgon, C.; Herres, N.; Vonlanthen, A.; Sigg, H. *J. Appl. Phys.* **2000**, *87*, 7825.

(9) Zollner, S. *J. Appl. Phys.* **2001**, *90*, 515.

(10) Carbone, F.; Gedik, N.; Lorenzana, J.; Zewail, A. H. *Advances in Condensed Matter Physics* **2010**, *2010*, 958618.

(11) Tao, Z.; Han, T. T.; Ruan, C.-Y *Phys. Rev. B* **2013**, *87*, 235124.

(12) Kittel, C. *Introduction to Solid State Physics*; Eds., Wiley: New York, 1986.

(13) Fushinobu, K.; Hijikata, H.; Majumdar, A. *J. Heat Trans.-T ASME* **1995**, *117*, 25-31.

(14) Joseph, D.D.; Preziosi, L. *Rev. Mod. Phys.* **1990**, *62*, 375-391.

(15) Chen G. *J. Heat Trans.* **2002**, *124*, 320-328.

(16) Schäfer, S.; Liang, W.; & Zewail, A. H. *Chem. Phys. Lett.* **2011**, *515*, 278-282.

(17) Luo, T.; Garg, J.; Shiomi, J.; Esfarjani, K.; Chen, G. *Europhys. Lett.* **2013**, *101*, 16001.

(18) Grange, T.; Ferreira, R.; Bastard, G. *Phys. Rev. B* **2007**, *76*, 241304(R).

(19) Maris, H.J.; Tamura, S. *Phys. Rev. B* **2012**, *85*, 054304.

(20) Siemens, M. E.; Li, Q.; Yang, R.; Nelson, K. A.; Anderson, E. H.; Murnane, M. M.; Kapteyn, H. C. *Nat. Mater.* **2010**, *9*, 26-30.

(21) Luckyanova, M. N.; Garg, J.; Esfarjani, K.; Jandl, A.; Bulsara, M. T.; Schmidt, A. J.; Minnich, A. J.; Chen, S.; Dresselhaus, M. S.; Ren, Z.; Fitzgerald, E. A.; Chen, G. *Science* **2012**, *338*, 936-939.

(22) Peraud, J.-P. M.; Hadjiconstantinau, N. G. *Appl. Phys. Lett.* **2012**, *101*, 153114.

(23) Swartz, E. T.; Pohl, R. O. *Rev. Mod. Phys.* **1989**, *61*, 605.